

Strain gauge measurement uncertainties on hydraulic turbine runner blade

J Arpin-Pont¹, M Gagnon¹, S A Tahan¹, A Coutu² and D Thibault³

¹Mechanical Engineering Department, École de technologie supérieure, 1100 Notre-Dame Street West, Montreal, QC H3C 1K3, Canada

²ANDRITZ-Hydro LTÉE, 6100, Trans-Canada Highway, Pointe-Claire, QC H9R 1B9, Canada

³Institut de recherche d'Hydro-Québec (IREQ), 1800 Boul. Lionel Boulet, Varennes, QC J3X 1S1, Canada

E-mail: jeremy.arpin-pont@gadz.org

Abstract. Strains experimentally measured with strain gauges can differ from those evaluated using the Finite Element (FE) method. This difference is due mainly to the assumptions and uncertainties inherent to each method. To circumvent this difficulty, we developed a numerical method based on Monte Carlo simulations to evaluate measurement uncertainties produced by the behaviour of a unidirectional welded gauge, its position uncertainty and its integration effect. This numerical method uses the displacement fields of the studied part evaluated by an FE analysis. The paper presents a study case using in situ data measured on a hydraulic turbine runner. The FE analysis of the turbine runner blade was computed, and our numerical method used to evaluate uncertainties on strains measured at five locations with welded strain gauges. Then, measured strains and their uncertainty ranges are compared to the estimated strains. The uncertainty ranges obtained extended from 74 $\mu\epsilon$ to 165 $\mu\epsilon$. Furthermore, the biases observed between the median of the uncertainty ranges and the FE strains varied from -36 to 36 $\mu\epsilon$. Note that strain gauge measurement uncertainties depend mainly on displacement fields and gauge geometry.

1. Introduction

In this paper, we introduce a numerical method to evaluate the uncertainties of strain measurements. Strains have a significant influence on mechanical analyses, such as lifetime estimation. Accurately determining strains and stresses is not as simple as it might seem. Experimental, analytical and numerical methods can be used to determine strain levels. Typical experimental methods involve the use of strain gauges to measure strains at specific locations on the surface of a part [1, 2]. In comparison, the Finite Element Method (FEM) is a numerical method used to estimate strain levels. Both methods have their respective simplifications which introduce uncertainties in the estimated strains. These uncertainties in turn can produce significant differences between the values estimated by FEM and those measured with strain gauges. The list of uncertainty sources is large, as shown in figure 1. In this paper, the uncertainties studied will be limited to the ones generated by the combination of the behavior of a welded gauge, its position uncertainty and its integration effect.

The proposed numerical method incorporates Monte Carlo simulations to evaluate the extent of these uncertainties. For each Monte Carlo simulation, the displacement fields estimated with FEM are

used to evaluate the strain measured by a virtual welded gauge located on the Finite Element model, and accounting for the studied uncertainties. The distribution of these strains determines the uncertainty range at the target gauge location.

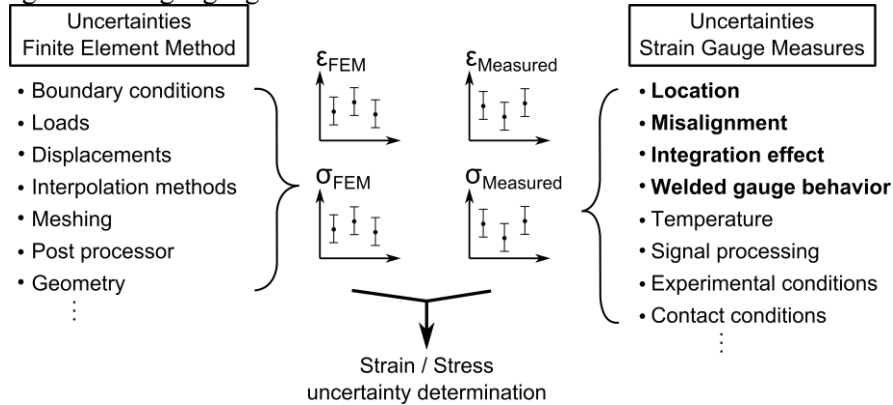


Figure 1. Uncertainties from FEM and Strain Gauge Measures.

Using the proposed methodology, the uncertainties of in situ data obtained on a hydraulic turbine runner were evaluated. The data from two runner blades instrumented with ten uniaxial welded strain gauges at five key locations were compared to the strains evaluated by FEM. To understand the differences observed between the two, we used our numerical method to estimate the uncertainty ranges around the estimated strains. For each gauge location, three strain values can be compared: the strain estimated by FEM at the target location, the strains of experimental measurements, and the strain distribution evaluated by virtual gauges placed on the FEM model and accounting for the studied uncertainties. Note that the proposed method is not specific to the sensor used, and could also be applied to other sensor geometries, types and other parts.

This paper is structured as follows: first, a review of the studied measurement uncertainty sources is presented. Next, our numerical method is introduced, and is followed by its application on a hydraulic turbine runner blade. Finally, a discussion on the results of the study case and the parameters influencing the uncertainty ranges concludes the paper.

2. Gauge measurement uncertainties

A bonded strain gauge is a sensor composed of an electrical wire forming grid lines on a matrix, as shown in figure 3. The electrical resistance of the wire is a function of its length, cross-sectional area and electrical resistivity. This type of gauge is glued directly on the part surface. When the part surface deforms, the gauge also deforms in the same manner; strain readings are obtained from the change in the electrical resistance of the electrical wire of the gauge due to its variations in length and cross-sectional area. The relation between the measured strain and the electrical resistance can be approximated by equation (1), where $\epsilon_{\text{Measured}}$ is the strain measured by the gauge following its longitudinal axis; K is the gauge factor (which is a function of the electrical wire material); and R and ΔR are the resistance and the resistance variation of the electrical wire, respectively [2].

$$\epsilon_{\text{Measured}} = \frac{1}{K} \frac{\Delta R}{R} \quad (1)$$

In his work, J. Pople [3] listed more than 70 uncertainty sources for strain gauge measurements. Most of them are linked to human factors, but others are inherent to the gauge technology. Uncertainties can be introduced during the positioning of the gauge at a target location, in which case the actual location might differ from the target location combined with an alignment error. Moreover, welded strain gauges behave differently from bonded strain gauges due to their construction. In this paper, the uncertainties produced by the gauge behavior, the location uncertainty which includes positioning and alignment errors, and the integration effect of a welded gauge are investigated. These

uncertainty sources are illustrated in figure 2. We consider the other uncertainty sources, presented in figure 1, as controlled or negligible.

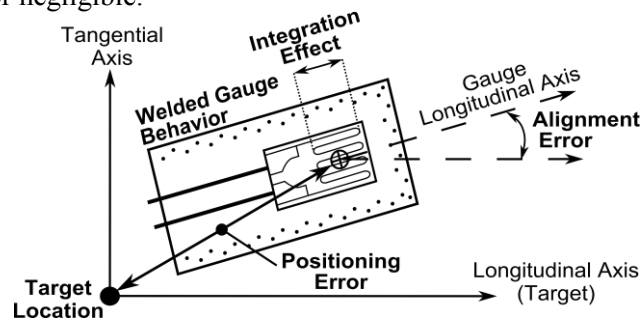


Figure 2. Definition of uncertainty sources: welded gauge behavior, location uncertainty (including positioning and alignment errors) and integration effect.

A unidirectional welded gauge possesses three main components: a thin carrier plate, a bonded gauge and connection cables [4]. The bonded gauge is glued on the thin carrier plate, which is then spot-welded on its periphery to the part surface, as shown in figure 4. Therefore, we obtain the strain measured on the carrier plate rather than the strain from the part surface. Displacement fields on the carrier plate can differ significantly from displacement fields on the part surface, leading to difference in strains and stresses. In our study, the uncertainty generated by the intermediate carrier plate is based on an FEM analysis of the carrier plate from which the displacement fields are obtained as a function of the gauge location. Note that welded gauges are easy to install on the part surface, are ready to use directly after their placement, and can be used in high temperature environments, where glues are not suitable [5].

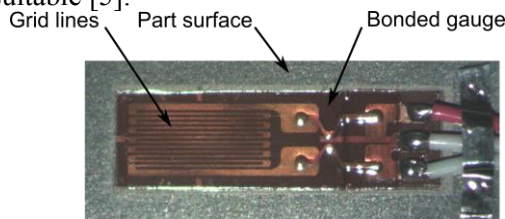


Figure 3. Bonded strain gauge.

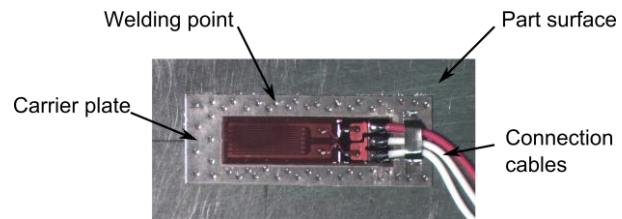


Figure 4. Welded strain gauge.

Experimentally, welded gauges are however difficult to accurately position at a target location and along a specific orientation, which produces positioning uncertainties. The displacement fields need to be known in order to evaluate the influence of these uncertainties but displacement fields are difficult to assess experimentally. We count few studies which examine the influence of positioning uncertainties [6, 7]. It should be noted that for a bonded gauge, the error on the strain produced by a misalignment in a uniform biaxial strain field was determined by C. Perry in 1969 [8]. This error is a function of three parameters: the ratio of the maximum-to-minimum algebraic principal strain; the angle between the gauge longitudinal axis and the maximum principal strain axis; and the alignment error of the gauge. The method proposed by C. Perry [8] is well adapted to bonded strain gauges but does not account for the behavior of the intermediate carrier plate of welded gauges. The method we propose uses the displacement fields of the carrier plate estimated by FEM and accounts for the positioning uncertainties to evaluate the strain measured by the gauge. These displacement fields also allow the evaluation of the integration error of the gauge.

A strain gauge does not measure the strain at its center, but integrates the strains under its active grid surface. Gafitanu *and al.* [9], and more recently, Younis and Kang [10], both developed different methods to evaluate this integration error. The error is a function of two factors: the size of the active grid of the gauge, and the strain gradient under the gauge, as shown in figure 5. According to Le Goër

and Avril [2] and Gafitanu *and al.* [9], the integration effect could generate a difference of 30% between the measured strain and the strain at the center point of the gauge.

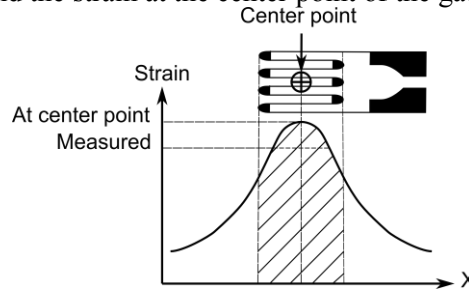


Figure 5. Influence of integration effect.

It should be noted that these uncertainties depend on the displacement fields in the neighborhood of the target location and the gauge geometry. In our study, the gauge geometry is known from specifications while displacement fields are estimated using an FEM model.

3. Numerical model

The numerical methodology developed in this study allows the estimation of the studied uncertainties using the displacement fields from the FEM. In our methodology, a Virtual Welded Gauge (VWG) is first generated numerically on the FEM surface. The VWG is positioned near the target location by accounting for positioning and alignment uncertainties. Since the accurate position of a gauge can be unknown during the experimental measurements, positioning uncertainties are generated using random distribution laws. These uncertainties determine an area around the target location in which the VWG can be positioned.

From the position of the VWG, displacements at the welding points on the periphery of the carrier plate are obtained by the interpolation of the displacement fields of the FEM surface. At welding points, the displacements of the carrier plate are assumed to be the same as those on the FEM surface. From these imposed displacements, a 2D FEM analysis of the carrier plate is computed. The rectangular carrier plate is meshed with 4-node shell elements. Nodes are positioned at the welding points on which the displacements are imposed. Therefore, the displacement fields obtained on the carrier plate can be compared to the displacement fields of the FEM part surface, as shown in figure 6. In this figure, a VWG is located on the FEM surface with positioning and alignment errors. The longitudinal displacement field isolines (mm) of the FEM surface and of the welded gauge carrier plate are plotted. We notice that even if the displacement fields are similar on the left side of the carrier plate, significant discrepancies are observed on the right. These discrepancies then influence the reading of the carrier plate strain gauge.

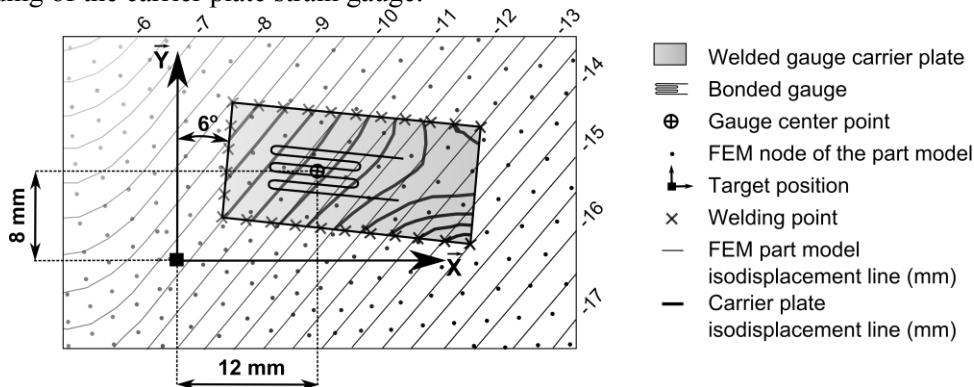


Figure 6. Virtual Welded Gauge created on an FEM part model surface. Positioning errors: 12 mm in longitudinal axis \bar{X} ; 8 mm in tangential axis \bar{Y} ; 6° angular. Longitudinal displacement fields U_X are plotted as isodisplacement lines (mm).

Using the displacement fields of the carrier plate, the strain measured by the VWG is evaluated by taking into account the gauge integration effect. In this case, the integration method on the all filaments length developed by Gafitanu *and al.* [9] is used. In this method, the strain from each grid line of the gauge ε_{gl_j} is determined with equation (2), where L_0 and L are respectively the initial and final length of the grid line j . \vec{U}_1 and \vec{U}_2 are the displacement vectors at the extremity points 1 and 2 of the grid line j , as shown in figure 7. These displacements are interpolated from the displacement fields of the 2D FEM model of the carrier plate. The final strain $\bar{\varepsilon}_{VWG}$ is estimated using equation (3), in which n is the number of grid lines of the gauge.

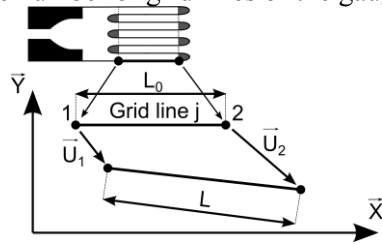


Figure 7. Strain determination for each grid line of the gauge.

$$\varepsilon_{gl_j} = \frac{\Delta L}{L_0} = \frac{L - L_0}{L_0} = \frac{\left[(L_0 + \vec{U}_2 \cdot \vec{X} - \vec{U}_1 \cdot \vec{X})^2 + (\vec{U}_2 \cdot \vec{Y} - \vec{U}_1 \cdot \vec{Y})^2 \right]^{1/2} - L_0}{L_0} \quad (2)$$

$$\bar{\varepsilon}_{VWG} = \frac{\sum_{j=1}^n \varepsilon_{gl_j}}{n} \quad (3)$$

Finally, Monte Carlo simulations are carried out to evaluate uncertainties. For each simulation, a VWG is generated next to the target location with random positioning uncertainties. The distribution of strains evaluated by the VWGs is computed and can be compared to the FEM strain at the target location, and to experimental values. Our assumption is that the difference observed between the median of the strain distribution obtained using our numerical method and the FEM strain at the target location can be assimilated to the bias observed between experimental measurements and original FEM analysis results. An overview of the methodology is presented in figure 8.

The method incorporates the following assumptions. We assume that the uncertainties observed are only due to the welded gauge behavior, the positioning uncertainties and the integration effect. These three sources of uncertainties depend on the displacement fields in the neighborhood of the target location. These displacement fields are estimated by FEM. However, because of the inherent uncertainties on FEM (see figure 1), the results cannot be considered to be exactly representative of actual displacement fields. This is combined with the assumption that displacements at the welding points of the carrier plate can be interpolated linearly from the displacement fields of the FEM surface. The displacements at the end of the grid lines are also interpolated linearly from the displacement fields of the carrier plate. It is assumed that the strain is uniform along each individual grid line of the gauge. Finally, the bonded gauge location on the carrier plate is known and the positioning uncertainties of the bonded gauge on the carrier plate are considered negligible.

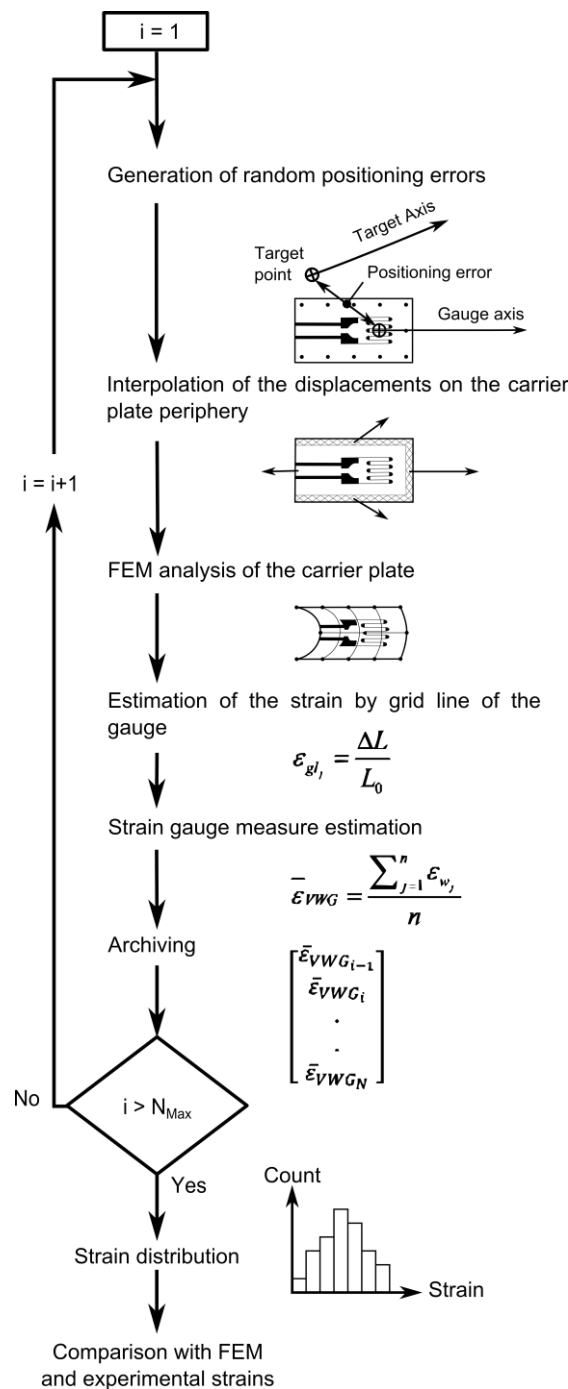


Figure 8. Method presentation.

4. Study case

The presented methodology was applied to experimental measurements made on a Francis hydraulic turbine runner. A total of ten (10) welded gauges were installed on two (2) blades. Each blade was instrumented at five (5) specific locations, as shown on the figure 9. At each location, strain distributions obtained with our numerical method are compared to FEM strain at the target location and experimental measurements.

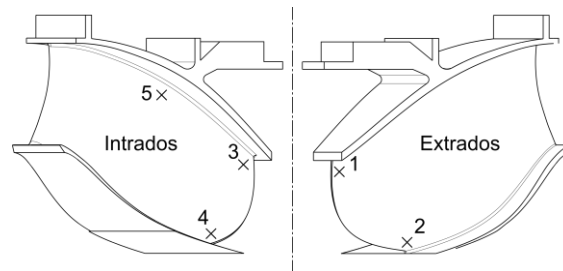


Figure 9. Position of the gauges placed on the hydraulic turbine blade during measurements.

The gauges used are referenced as HBW-35-250-6-UP (Hitec Products Inc.). The distribution laws used to generate positioning and alignment errors were the same for the five locations, and are presented in table 1. These random position laws were estimated from the results of a Reproducibility and Reliability analysis (R&R) realized on a similar runner. This analysis was conducted using several strain gauges repeatedly installed at specific locations, following the experimental conditions of our reference project. Each time a gauge was installed, its positioning errors were accurately measured, and the gauge was removed. The process was repeated until the parameters of the distribution of the positioning uncertainties could be estimated

Table 1. Positioning uncertainty distribution laws used for the simulations.

Uncertainty	Distribution	Parameters
Position along target axis \bar{X} (mm)	Uniform	[-10; 10]
Position along tangential axis \bar{Y} (mm)	Uniform	[-6; 6]
Alignment angle ($^{\circ}$)	Uniform	[-5; 5]

Furthermore, sensibility analyses were carried out to determine the influences of the number of elements in the 2D FEM of the carrier plate and the Monte Carlo simulation number. Stability is obtained with 400 elements and 2×10^3 Monte Carlo simulations. For the study case, we meshed the carrier plate with 551 rectangular elements (30 nodes in length and 20 nodes in width of the carrier plate) and computed uncertainties using 5×10^3 Monte Carlo simulations.

5. Results

The strain results obtained are shown in figure 10, with detailed results for each location in table 2.

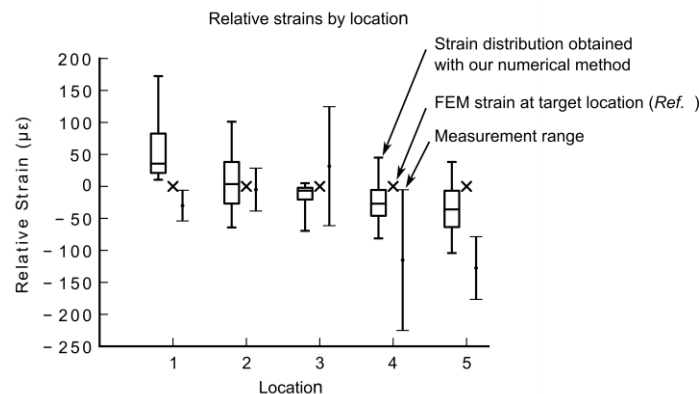


Figure 10. Strain distributions resulting from 5×10^3 Monte Carlo simulations and experimental strain ranges for each of the five locations. Strains are expressed relative to the FEM strain at the target location.

Table 2. Relative strain results.

Location	Numerical method strain results (Microstrain $\mu\epsilon$)					Measurement range ($\mu\epsilon$)	
	Median ($Q_{50\%}$)	[$Q_{25\%}$; $Q_{75\%}$]	(range)	[Min; Max]	(range)	[Min; Max]	(range)
1	36	[21; 83]	(62)	[10; 172]	(162)	[-54; -6]	(48)
2	4	[-27; 38]	(65)	[-64; 101]	(165)	[-38; 29]	(67)
3	-7	[-20; -2]	(18)	[-69; 5]	(74)	[-61; 125]	(186)
4	-27	[-46; -6]	(40)	[-81; 45]	(126)	[-225; -5]	(220)
5	-36	[-64; -7]	(57)	[-104; 38]	(142)	[-177; -79]	(98)

The relative strains represent the difference between the strains obtained and the expected strain from the FEM at the target location. The boxes represent the first and third quartile ($Q_{25\%}$ and $Q_{75\%}$) of the relative strain distribution obtained with our numerical method, the middle line is the median ($Q_{50\%}$), and whiskers extend to the extreme values. The measurement ranges are the interval formed by strains observed during measurements. Measured strains were established from three independent measurements made at similar operating conditions. We observe an offset between the calibration values of each measurement, which produces variations in measured strains. Moreover, for each location, two different blades were instrumented. The strain measurement ranges presented in this study include the variations observed between both blades and the three independent measurements. Their statistical distributions, however, have not been determined.

6. Discussion

We observe three different result combinations. The first, observed at location 1, is that the strain distribution obtained with our numerical method and the experimental measure range do not overlap. At this location, the FEM strain estimated at the target location is outside the measurement range. The uncertainties estimated with our method cannot explain this difference. In this case, it is possible that assumptions on both FEM and experimental measurements are false. The second combination, observed at locations 2, 3 and 4, is that more than 50% of the strains obtained with our numerical method overlap with the experimental measurement range. For location 4, the FEM strain at the target location is out of the experimental strain range, but the strain distribution estimate with our numerical method cover both the initial FEM results and part of the measurement range. Thus, the studied uncertainties could be considered as a cause of the differences between the FEM strain and experimental strains. A third possibility is observed for location 5. For this gauge, only a small part of the strains estimated with our numerical method overlap with the measurement range. The difference between the FEM strain at the target location and the nearest measured strain is $79 \mu\epsilon$. We observe that the strain distribution obtained with the numerical method, including the calculated uncertainties, shifted to the same side as the experimental measurements, which can only partially explain the differences observed between FEM and experimental strains.

Strain distributions estimated by the virtual welded gauges are directly dependent on the FEM displacement fields around the target location. The geometry of the welded gauge, including the sizes of the carrier plate and of the bonded gauge, are determinant factors in the estimation of the welded gauge behavior error and the integration error. The random distribution laws used to generate the positions of virtual welded gauges are also important due to the importance of the FEM displacement fields. Uncertainty ranges obtained in this study case vary from 74 to $165 \mu\epsilon$ for locations 3 and 2, respectively. The biases of the relative strains obtained vary from -36 to $36 \mu\epsilon$ for locations 5 and 1,

respectively. Results are specific to each location and the numerical method has to be applied at each location independently in order to estimate the measurement uncertainties.

7. Conclusions

In this paper, we have presented a numerical method, which enables the estimation of measurement uncertainties due to welded gauge behavior, positioning uncertainties and integration effect in strain measurement with welded strain gauges. In this method, the uncertainty ranges are estimated using the part surface displacement fields evaluated with an FEM analysis. Using these displacement fields, Monte Carlo simulations are carried out to estimate the distribution of strains estimated by virtual welded gauges randomly placed in the neighborhood of the target location on the FEM surface. The obtained distribution allows the estimation of the measurement uncertainty ranges. When applied to in situ measurements carried out on hydraulic turbine runner blades, uncertainty ranges obtained extend from 74 to 165 $\mu\epsilon$, while biases vary from -36 $\mu\epsilon$ to 36 $\mu\epsilon$. We observe that in some cases, the differences between experimental measured strains and strains evaluated by FEM cannot be explained by our simulation results. In these cases, we consider that the observed differences are due to the assumptions of both FEM analysis and experimental measurements. In most cases, the studied uncertainty could explain the differences between experimental measured strains and FEM strains. However, our numerical method does not include all the measurement uncertainty sources: uncertainties due to the transverse sensitivity of the gauge, the temperature compensation or the signal processing are not taken in account. Moreover, actual geometrical and load differences between the finite element model and the real runner are not considered either. We believe, however, that the two main factors influencing the measurement uncertainty sources are the displacement fields and the gauge geometry.

Acknowledgments

This study was carried out with the financial support of the Canadian research internship program, Mitacs-Accelerate. The authors acknowledge Andritz Hydro Ltd., the Institut de Recherche d'Hydro-Québec (IREQ) and the École de technologie supérieure (ÉTS) for their support, materials and advice.

Nomenclature

K	Gauge factor	ΔL	Length variation [mm]
L_0	Initial gauge grid line length [mm]	ΔR	Gauge resistance variation [Ω]
L	Final gauge grid line length [mm]	$\epsilon_{\text{Measured}}$	Strain measured by the gauge [$\mu\epsilon$]
n	Number of grid lines of the gauge	ϵ_{gl_j}	Estimated strain for the grid line j [$\mu\epsilon$]
R	Gauge resistance [Ω]	$\bar{\epsilon}_{\text{VWG}}$	Estimated strain for the Virtual Welded Gauge [$\mu\epsilon$]
\vec{U}_i	Displacement vector of point i [mm]	$\mu\epsilon$	Microstrain [mm/mm x 10^6]

References

- [1] James W F R and Dally W 1991 *Experimental Stress Analysis* 3rd ed (New-York: McGraw-Hill College Division)
- [2] Le Goër J L and Avril J 1992 Extensométrie *Techniques de l'ingénieur* R **1850** 17
- [3] Pople J 1984 *Experimental Techniques* **8-9** 34-38
- [4] Vishay Micro-Measurements 2010 Special use sensors – weldable strain gages *Standard Weldable Patterns* Document Number **11519**
- [5] Avril J 1984 *Encyclopédie d'analyse des contraintes* (Malakoff: Micromesures)
- [6] Little E G, Ticher D, Colgan D and O'Donnell P 2006 *Strain* **42** 207-16
- [7] Kobayoshi M and Queenie S H C 2005 *Measurement* **38** 67-76
- [8] Perry C 1969 *Instruments and control systems* **42-10** 137-39
- [9] Gafitanu M, Barsanescu P D and Poterasu V F 1989 *Int. J. Pres. Ves & Piping* **41** 127-39

- [10] Younis N T and Kang B 2011 *Journal of Mechanical Science and Technology* **25-1** 163–169

Reproduced with permission of copyright owner. Further reproduction prohibited without permission.